Nonlinear Dyn (2018) 93:2565–2578
https://doi.org/10.1007/s11071-018-4342-7

ORIGINAL PAPER

Modal damping variations in nonlinear dynamical systems

Mohammad A. AL-Shudeifat

Received: 9 January 2018 / Accepted: 30 April 2018 / Published online: 14 May 2018

Abstract For any linear dynamical system coupled with one or more nonlinear dynamical attachments, the effect of nonlinear energy content on modal damping variations of the entire system has not been clearly addressed in the literature. Accordingly, a novel method is employed here to formulate the amplitude-dependent modal damping matrix for such nonlinear dynamical systems using an amplitude-dependent stiffness approach. The proposed method is directly applied into the equations of motion where numerical and analytical solutions are not required to be known a priori. This advantage is highly desirable to study the dynamical behavior of nonlinear dynamical systems by direct application of methods into equations of motion. Accordingly, the modal damping content variations under the effect of amplitude-dependent stiffness are investigated here. The method is based on linearizing the nonlinear coupling stiffness where a scaled amplitude-dependent stiffness has been obtained to replace the original nonlinear coupling stiffness in the system. Accordingly, the amplitude-dependent modal damping matrix in modal coordinates is obtained and investigated. Consequently, new significant findings regarding modal damping content variations under the effect of the change in nonlinear energy during oscillation are achieved through this study. Furthermore, the nonlinear amplitude-dependent modal damping matrix of the equivalent system is found to be satisfying all matrix similarity conditions with the linear amplitude-independent modal damping matrix of the original system. These findings are expected to be of significant impact on passive nonlinear targeted energy transfer for shock mitigation and energy-harvesting fields.

Keywords Nonlinear dynamical systems · Frequency-energy dependence · Nonlinear frequency · Nonlinear stiffness · Nonlinear modal damping content

M. A. AL-Shudeifat (✉)
Aerospace Engineering, Khalifa University of Science and Technology, Abu Dhabi, UAE
e-mail: mohd.shudeifat@kustar.ac.ae

1 Introduction

Appearance of nonlinear coupling stiffness components in single- or multi-degree-of-freedom linear dynamical systems significantly affects the dynamical behavior of such systems. Most of the studies in the literature have focused on introducing different methods for obtaining frequency-energy dependence and approximate solutions to conservative and non-conservative nonlinear oscillators.

For all nonlinear dynamical systems, the frequencies become amplitude- and energy-dependent quantities. The dynamical behavior of nonlinear frequencies has been well studied via various analytical and numerical techniques in the literature, especially through the frequency-energy plots (FEPs) [1–5]. These FEPs have been obtained via numerical integration continuation methods where the underlying dynamic in the considered systems has been clearly revealed through these

FEPs. The conservative versions of nonlinear systems were usually considered for studying the nonlinear frequency content. For such conservative dynamical systems, like the duffing oscillator or any linear system attached to it, several analytical and numerical methods were also proposed to study the nonlinear frequency-energy behavior in such systems [6–19]. The most common methods employed in the literature to approximate frequencies and periodic solutions of these systems are the perturbation and multiple-timescale methods [6,7]. In addition, the harmonic balance method in [6–13], homotopy perturbation method [14–16], and Krylov–Bogoliubov [17] were also employed with such nonlinear oscillators. Most of these studies have focused on the odd-power stiffness components in the nonlinear coupling force in single- or multi-degree-of-freedom undamped systems. However, for the damped nonlinear systems with odd-power stiffness components, several studies have provided excellent approximations for the solutions, nonlinear frequencies, and the amplitudes decays [17–24]. The coupling force with non-negative real-power stiffness components in nonlinear system has been addressed in another series of publications for conservative and neoconservative systems [25–29]. In these studies, methods of solutions and amplitudes decay relations were introduced. However, finding exact solutions for non-conservative nonlinear dynamical systems is still a challenging task in the field, especially for multi-degree-of-freedom nonlinear dynamical systems.

It is highly desirable to introduce analytical methods that can be directly applied into equations of motion of non-conservative nonlinear dynamical systems where numerical simulation response is not required to be obtained a priori. However, the need of introducing a methodology to study the effect of nonlinear stiffness components in dynamical systems on their entire modal damping content during oscillation is one of challenging problems in nonlinear dynamics. Therefore, the exact scaling parameter derived in [30,31] has made it possible to develop a method to study the effect of incorporating nonlinear stiffness components in linear dynamical systems on their modal damping content during oscillation. This scaling parameter was originally derived to replace the original nonlinear stiffness by an exact equivalent time-dependent stiffness to generate plots of frequency versus nonlinear energy content where numerical simulation response was required for the method application. Here, the method is further developed to become amplitude-dependent stiffness rather than time-dependent stiffness where numerical simulation is not required to be known a priori. Consequently, the amplitude-dependent modal damping matrix of the entire nonlinear dynamical system becomes obtainable. Consequently, the obtained modal damping coefficients are plotted with respect to nonlinear energy content in the system to investigate the effect of nonlinear stiffness components on the full system. Significant findings and mathematical relationships have been reached through this study regarding modal damping content variations which are expected to be of noticeable impact on nonlinear targeted energy transfer (TET) fields (i.e., shock mitigation and nonlinear energy harvesting) and other nonlinear dynamical applications.

2 Method description

In [30], a time-dependent stiffness method was proposed for extracting backbone branches in the frequency-nonlinear-energy plot (FNEP) where numerical solution was required to be employed with the method. Here, the method is further developed to be amplitude-dependent stiffness method rather than time-dependent stiffness method. Therefore, it becomes directly applied into equations of motion where numerical integration of equations of motion is not required to be known a priori. Accordingly, the nonlinear coupling stiffness is replaced here by a scaled amplitude-dependent stiffness rather than time-dependent stiffness. This modification has made it possible here to replace the original nonlinear dynamical system at each amplitude in the nonlinear spring by an equivalent amplitude-dependent linear system. Therefore, the transformation into modal coordinates at each amplitude in the nonlinear spring is directly obtained to study the variations of modal damping content in the original nonlinear system. It is found that in [30] there should be a scaling parameter to preserve the equivalency between potential energies of the amplitude-dependent linearized coupling force and the original nonlinear force. Otherwise, direct replacement of the nonlinear coupling stiffness with amplitude-dependent stiffness at each amplitude in the nonlinear spring does not preserve the equivalency between potential energies without that scaling parameter. Obtaining such scaling parameter has made it possible to linearize the nonlinear coupling force, which

makes the method to be directly applied into the equations of motion. This parameter has been represented by δ, and its mathematical formula was obtained in [30] as

$$\delta = \frac{2}{\pi\,(p+1)} \left(\frac{\Gamma\left(\frac{1}{p+1}\right)}{\Gamma\left(\frac{p+3}{2(p+1)}\right)} \right)^2 \tag{1}$$

where $\delta = 1$ only for $p = 1$. Otherwise, $\delta > 1$ for $p > 1$.

For the application of the proposed method to study the modal damping content in nonlinear systems, the duffing equation of purely odd-power stiffness restoring force is firstly reconsidered here for more demonstration, which is expressed as

$$m\ddot{z} + \lambda\dot{z} + k_{\mathrm{nl}} z^p = 0, \tag{2}$$

where λ is the damping coefficient, k_{nl} is the nonlinear stiffness coefficient, and p is a nonnegative odd power. Therefore, the nonlinear force in Eq. (2) is replaced by an equivalent scaled amplitude-dependent stiffness $k\,(Z)\,Z$ at each value of Z (amplitude change in the nonlinear spring) of the nonlinear spring as

$$\frac{k_{\mathrm{nl}}}{\delta} Z^P \equiv k\,(Z)\,Z \tag{3}$$

Therefore, the exact amplitude-dependent frequency in [26] is rewritten in terms of δ and Z as

$$\Omega\,(Z) = \sqrt{\frac{k_{\mathrm{nl}}}{m\delta}} Z^{\left(\frac{p-1}{2}\right)} \tag{4}$$

Now, it becomes possible at each value of Z to represent the amplitude-dependent stiffness by

$$k\,(Z) = \frac{1}{\delta} k_{\mathrm{nl}} Z^{P-1} \text{ where } \Omega\,(Z) = \sqrt{\frac{k\,(Z)}{m}} \tag{5}$$

The amplitude-dependent equivalent system to the original system in Eq. (2) is now expressed in either of the following equations

$$\begin{aligned} &m\ddot{z} + \lambda\dot{z} + \delta\, k\,(z)\, z = 0 \\ &\ddot{z} + \alpha\dot{z} + \delta\, \Omega^2\,(z)\, z = 0 \end{aligned} \tag{6}$$

where $\alpha = \lambda/m$. This equivalent amplitude-dependent system actually preserves the exact frequency content and response of the original system in Eq. (2). The numerical simulation responses of the original system in Eq. (2) and the equivalent system in Eq. (6) are shown in Fig. 1 for an arbitrary physical parameters set of $m = 20$ kg, $\lambda = 2$ N s/m, $k_{\mathrm{nl}} = 6000$ N/m^3, and $p = 3$. Therefore, the equivalent system is found retrieving the exact response and frequency of the original system as shown at $\delta = 1.3932$.

3 Application with nonlinear multi-degree-of-freedom dynamical systems

The proposed amplitude-dependent stiffness method is applied to a multi-degree-of-freedom linear system coupled with a nonlinear attachment as shown in Fig. 2. Accordingly, for the relative displacement $Z = x_N - x_{N-1}$ between the masses M_{N-1} and m, the nonlinear coupling stiffness is replaced by $k\,(Z)$ according to Eq. (5). Therefore, the amplitude-dependent stiffness matrix of the system is updated at each value of Z as

$$\mathbf{K}_{\mathrm{eq}}\,(Z) = \begin{bmatrix} k_1 + k_2 & -k_1 & & & & & \\ -k_1 & k_2 + k_3 & -k_3 & & & 0 & \\ & \ddots & \ddots & \ddots & & & \\ & & -k_j & k_j + k_{j+1} & -k_{j+1} & & \\ & & & \ddots & \ddots & \ddots & \\ & 0 & & & -k_{N-1} & k_{N-1} + k\,(Z) & -k\,(Z) \\ & & & & & -k\,(Z) & k\,(Z) \end{bmatrix} \tag{7}$$

Consequently, for each value of Z in a selected range of initial relative amplitudes between the masses M_{N-1} and m, the corresponding modal matrix $\mathbf{\Phi}\,(Z)$ is

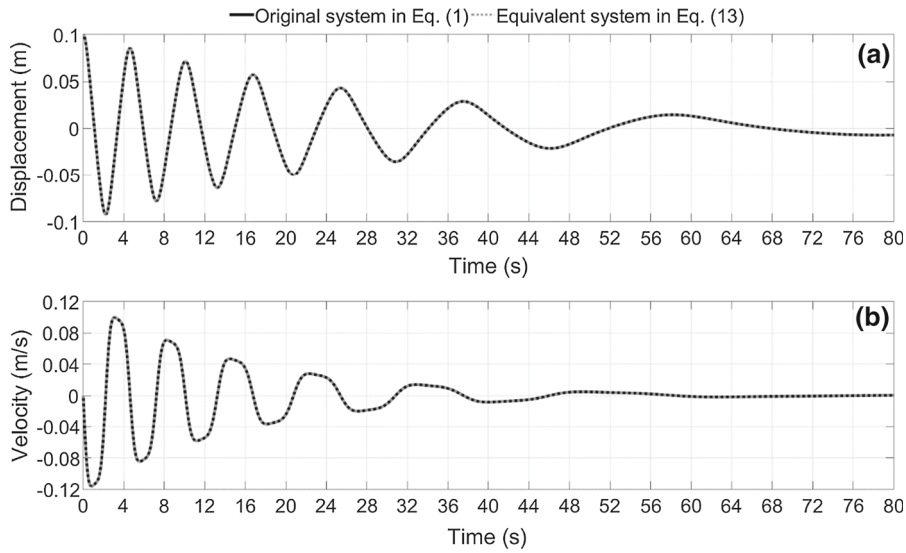

Fig. 1 Comparison between the responses of the exact system in Eq. (2) and its equivalent amplitude-dependent stiffness system in Eq. (6) at $\delta = 1.3932$

obtained from the eigensolution of $\mathbf{M}^{-1/2}\mathbf{K}(Z)\,\mathbf{M}^{-1/2}$. Therefore, the amplitude-dependent frequencies of the fundamental backbone branches of the system are obtained from

$$\boldsymbol{\Omega}(Z) = \left(\boldsymbol{\Phi}(Z)^{\mathrm{T}}\,\mathbf{M}^{-1/2}\mathbf{K}(Z)\,\mathbf{M}^{-1/2}\boldsymbol{\Phi}(Z)\right)^{1/2} = \begin{bmatrix} \Omega_1(Z) & & & & \\ & \Omega_2(Z) & & 0 & \\ & & \ddots & & \\ & & & \Omega_j(Z) & \\ & & & & \ddots \\ & 0 & & & \Omega_{N-1}(Z) \\ & & & & & \Omega_N(Z) \end{bmatrix} \tag{8}$$

The corresponding amplitude-dependent modal damping matrix is obtained as

$$\lambda(Z) = \boldsymbol{\Phi}(Z)^{\mathrm{T}}\,\mathbf{M}^{-1/2}\mathbf{D}\mathbf{M}^{-1/2}\boldsymbol{\Phi}(Z) \tag{9}$$

where $\mathbf{D}$ is the linear physical damping matrix of the original system (including λ_N) .

4 Application with LO-NES system

The method is applied here to the two-degree-of-freedom system shown in Fig. 3. This system is composed of a linear oscillator (LO) and a nonlinear energy sink (NES). The NES is a small coupled mass to the linear system that performs a nonlinear targeted energy transfer (TET) [1] of significant portion of the input energy induced into the linear structure to be dissipated by its local damping. The considered LO-NES system in Fig. 3 is governed by the following equations of motion:

$$\begin{bmatrix} M & 0 \\ 0 & m \end{bmatrix}\begin{bmatrix} \ddot{u} \\ \ddot{v} \end{bmatrix} + \begin{bmatrix} \lambda_1+\lambda_2 & -\lambda_2 \\ -\lambda_2 & \lambda_2 \end{bmatrix}\begin{bmatrix} \dot{u} \\ \dot{v} \end{bmatrix} + \begin{bmatrix} k_1 & 0 \\ 0 & 0 \end{bmatrix}\begin{bmatrix} u \\ v \end{bmatrix} + \begin{bmatrix} -k_{\mathrm{nl}}(v-u)^p \\ k_{\mathrm{nl}}(v-u)^p \end{bmatrix} = \begin{bmatrix} 0 \\ 0 \end{bmatrix} \tag{10}$$

where

$$\mathbf{M} = \begin{bmatrix} M & 0 \\ 0 & m \end{bmatrix}, \quad \mathbf{D} = \begin{bmatrix} \lambda_1+\lambda_2 & -\lambda_2 \\ -\lambda_2 & \lambda_2 \end{bmatrix} \text{ and } \mathbf{q} = \begin{bmatrix} u \\ v \end{bmatrix}$$

According to Eq. (5), the amplitude-dependent stiffness matrix in Eq. (7) is rewritten for this LO-NES

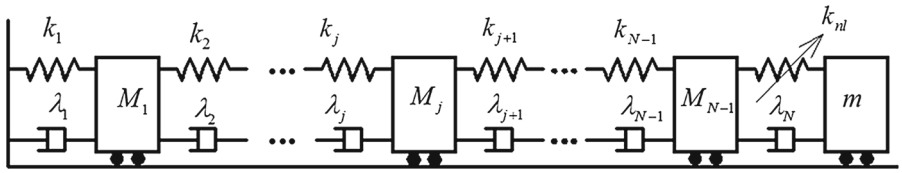

Fig. 2 Multi-degree-of-freedom discrete spring-mass system coupled with a nonlinear attachment

system as

$$\mathbf{K}_{\text{eq}}(Z) = \begin{bmatrix} k_1 + k(Z) & -k(Z) \\ -k(Z) & k(Z) \end{bmatrix} \tag{11}$$

where $k(Z)$ is calculated by $k(Z) = k_{\text{nl}} Z^{P-1}/\delta$ for the preselected range of relative displacements between the LO and the NES masses (i.e., $Z = v - u$). The instantaneous amplitude-dependent natural frequencies and damping coefficients are, respectively, obtained in modal coordinates at each value of Z as

$$\begin{aligned} \boldsymbol{\Omega}_{\text{nl}}(Z) &= \left(\boldsymbol{\Phi}(Z)^{\text{T}}\ \mathbf{M}^{-1/2}\mathbf{K}(Z)\,\mathbf{M}^{-1/2}\boldsymbol{\Phi}(Z)\right)^{1/2} \\ &= \begin{bmatrix} \Omega_1(Z) & 0 \\ 0 & \Omega_2(Z) \end{bmatrix} \end{aligned} \tag{12a}$$

$$\begin{aligned} \boldsymbol{\lambda}_{\text{nl}}(Z) &= \begin{bmatrix} \lambda_{\text{nl},11}(Z) & \lambda_{\text{nl},12}(Z) \\ \lambda_{\text{nl},21}(Z) & \lambda_{\text{nl},22}(Z) \end{bmatrix} \\ &= \boldsymbol{\Phi}(Z)^{\text{T}}\ \mathbf{M}^{-1/2}\mathbf{D}\mathbf{M}^{-1/2}\boldsymbol{\Phi}(Z) \end{aligned} \tag{12b}$$

Therefore, the equivalent system of amplitude-dependent stiffness and amplitude-dependent modal damping matrices is expressed in modal coordinates as

$$\begin{bmatrix} 1 & 0 \\ 0 & 1 \end{bmatrix} \begin{bmatrix} \ddot{y}_1 \\ \ddot{y}_2 \end{bmatrix} + \begin{bmatrix} \lambda_{\text{nl},11}(Z) & \lambda_{\text{nl},12}(Z) \\ \lambda_{\text{nl},21}(Z) & \lambda_{\text{nl},22}(Z) \end{bmatrix} \begin{bmatrix} \dot{y}_1 \\ \dot{y}_2 \end{bmatrix} + \begin{bmatrix} \Omega_1^2(Z) & 0 \\ 0 & \Omega_2^2(Z) \end{bmatrix} \begin{bmatrix} y_1 \\ y_2 \end{bmatrix} = \begin{bmatrix} 0 \\ 0 \end{bmatrix} \tag{13}$$

where $\mathbf{y} = [y_1\ \ y_2]^{\text{T}} = \boldsymbol{\Phi}(Z)^{\text{T}}\mathbf{M}^{1/2}[u\ \ v]^{\text{T}}$ and $\boldsymbol{\Phi}(Z)$ is the amplitude-dependent modal matrix obtained at each value of Z from the eigensolution of $\mathbf{M}^{-1/2}\mathbf{K}(Z)\,\mathbf{M}^{-1/2}$. The obtained instantaneous frequencies from Eq. (12a) can be used to generate the fundamental backbones of the system where these frequencies are plotted with respect to the corresponding nonlinear potential energies in the nonlinear coupling spring which is given by

$$E_{\text{pe}}^{\text{nl}}(Z) = \frac{k_{\text{nl}}}{p+1} Z^{P+1} \tag{14}$$

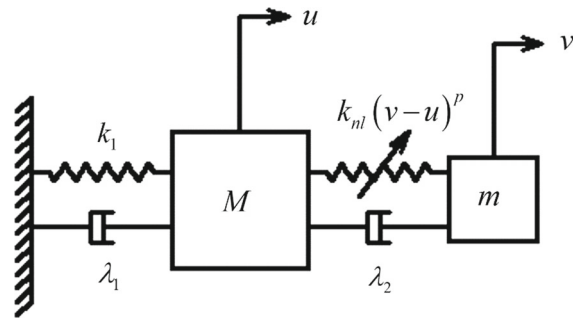

Fig. 3 Linear oscillator (LO) coupled with a nonlinear energy sink (LO-NES system)

To study the robustness of the proposed method in predicting the effect of nonlinear energy content in the nonlinear spring on amplitude-dependent modal damping variations, an arbitrary physical parameters of the considered LO-NES system in Fig. 3 are selected for both analytical and numerical analyses as $M = 1$ kg, $k_1 = 1$ N/m, $\lambda_1 = 0.02$ N · s/m, $m = 0.05$ kg, $\lambda_2 = 0.002$ N · s/m, $k_{\text{nl}} = 1$ N/m^3, and $p = 3$. At $p = 3$, the value of the scaling parameter is found here to be $\delta = 1.3932$. Accordingly, the exact nonlinear force $k_{\text{nl}}(v-u)^p$ at each value of $Z = v - u$ is replaced by the equivalent scaled amplitude-dependent stiffness force for both analytical and numerical investigations as $k(Z)\,Z = \frac{k_{\text{nl}}}{\delta} Z^P = 0.71777 k_{\text{nl}} Z^P$, where $k(Z) = 0.71777 k_{\text{nl}} Z^{P-1}$. In addition, the system in Fig. 3 is also considered with the previously given physical parameters for the linear case of $p = 1$ by assuming $k_1 \equiv k_{\text{nl}}$ in the numeric value. For this reference system, the amplitude-dependent modal matrix is obtained as

$$\begin{aligned} \boldsymbol{\lambda}_{\text{Lin}}(Z) &= \boldsymbol{\Phi}(Z)^{\text{T}}\ \mathbf{M}^{-1/2}\mathbf{D}\mathbf{M}^{-1/2}\boldsymbol{\Phi}(Z) \\ &= \begin{bmatrix} \lambda_{\text{Lin},11}(Z) & \lambda_{\text{Lin},12}(Z) \\ \lambda_{\text{Lin},21}(Z) & \lambda_{\text{Lin},22}(Z) \end{bmatrix} \\ &= \begin{bmatrix} 0.0190 & 0.0040 \\ 0.0040 & 0.0430 \end{bmatrix} \end{aligned} \tag{15}$$

The above damping matrix is an amplitude-independent modal damping matrix since for $p = 1$ the system is linear. However, for $p = 3$, both stiffness and damp-

ing matrices become amplitude-dependent matrices as previously given in Eq. (12). The amplitude Z in the nonlinear coupling spring is now varied for the range $0 \leq Z \leq 4$, where for each value of Z, Eqs. (11), (12), and (14) are evaluated to generate the results in Fig. 4, of which the numerical simulation solution is not required. In this figure, the damping coefficients obtained from Eq. (12b) for $p = 3$ and from Eq. (15) for $p = 1$ are plotted. It is discovered by this figure that the modal damping content in the nonlinear system is strongly affected by the nonlinear potential energy variations during the NES mass oscillation. In addition, when the relative displacement of the NES mass is high, the instantaneous damping content in the LO-NES system gets closer to that of the corresponding reference linear system at $k_1 \equiv k_{\text{nl}}$. However, the damping content in the LO-NES system starts to significantly deviate from that of the corresponding reference linear system at intermediate and low relative displacements of the NES as shown. This figure is named here as modal damping nonlinear energy plot (MDNEP).

The observations in Fig. 4 are further investigated in Figs. 5 and 6. The sums of diagonal damping coefficients in $\boldsymbol{\lambda}_{\text{Lin}}(Z)$ for $p = 1$ of the reference linear system and for $\boldsymbol{\lambda}_{\text{nl}}(Z)$ for $p = 3$ of the nonlinear system are found to be exactly equal according to Fig. 5a and the corresponding error calculation in Fig. 5b. It is also found that the determinants of the modal damping matrices of both linear reference system in Eq. (15) and the nonlinear system in Eq. (12b) are exactly equal according to the results shown in Fig. 6a and the corresponding error calculation in Fig. 6b. Therefore, it is interesting to find out that the nonlinear amplitude-dependent modal damping matrix $\boldsymbol{\lambda}_{\text{nl}}(Z)$ satisfies all matrix similarity conditions with the constant amplitude-independent linear modal damping matrix $\boldsymbol{\lambda}_{\text{Lin}}(Z)$ such that both matrices have similar determinant, trace (the sum of diagonal elements), rank, and eigenvalues. These findings yield a mathematical equation of a circle at which plot of diagonal damping coefficients against the anti-diagonal damping coefficient appears. Accordingly, the related mathematical relations are obtained as

$$\begin{aligned}
&\lambda_{\text{nl},11} + \lambda_{\text{nl},22} = \lambda_{\text{Lin},11} + \lambda_{\text{Lin},22} \\
&R_\lambda = \frac{1}{2}\sqrt{\left(\lambda_{\text{Lin},22} - \lambda_{\text{Lin},11}\right)^2 + 4\lambda_{\text{Lin},12}^2} \\
&C_\lambda = \frac{1}{2}\left(\lambda_{\text{Lin},11} + \lambda_{\text{Lin},22}\right) \\
&\left(\lambda_{\text{nl},11}^{-} C_\lambda\right)^2 + \lambda_{\text{nl},12}^2 = R_\lambda^2 \\
&\left(\lambda_{\text{nl},22}^{-} C_\lambda\right)^2 + \lambda_{\text{nl},12}^2 = R_\lambda^2
\end{aligned} \tag{16}$$

where R_λ and C_λ are the radius and the center of the damping projection circle, respectively. Consequently, for the given physical parameters of the system in Fig. 3, the following mathematical relations between the reference linear system modal damping and the amplitude-dependent modal damping of the nonlinear system for any initial condition are obtained as

$$\begin{aligned}
&R_\lambda = \frac{1}{2}\sqrt{\left(\lambda_{\text{Lin},22} - \lambda_{\text{Lin},11}\right)^2 + 4\lambda_{\text{Lin},12}^2} = 0.0123 \\
&C_\lambda = \frac{1}{2}\left(\lambda_{\text{Lin},11} + \lambda_{\text{Lin},22}\right) = 0.031 \\
&\lambda_{\text{nl},11} + \lambda_{\text{nl},22} = 0.062 \\
&\left(\lambda_{\text{nl},11}^{-} 0.031\right)^2 + \lambda_{\text{nl},12}^2 = 1.52 \times 10^{-4} \\
&\left(\lambda_{\text{nl},22}^{-} 0.031\right)^2 + \lambda_{\text{nl},12}^2 = 1.52 \times 10^{-4}
\end{aligned} \tag{17}$$

To verify relation Eq.(17), the diagonal damping coefficients are plotted against the anti-diagonal damping coefficient in $\boldsymbol{\lambda}_{\text{Lin}}(Z)$ for $p = 1$ of the linear system and in $\boldsymbol{\lambda}_{\text{nl}}(Z)$ for $p = 3$ of the nonlinear system where these plots coincide with the exact circle obtained from Eq. (17) as shown in Fig. 7.

The above findings are further verified here for the system at $p = 1$ and $p = 3$ via numerical simulation response. The response of displacements and velocities of the LO-NES system are obtained via numerical simulation for the previously given physical parameters at $u(0) = 0$, $v(0) = 4$, and $\dot{u}(0) = \dot{v}(0) = 0$. The relative displacement Z is evaluated at each time step according to the exact values of $u(t)$ and $v(t)$ obtained by numerical integration, where $Z = u(t) - v(t)$. At each value of Z, Eqs. (11), (12), (14) are again evaluated according to the numerical simulation response. Consequently, the obtained numerical simulation diagonal damping coefficients are plotted against the anti-diagonal coefficient in $\boldsymbol{\lambda}_{\text{nl}}(Z)$ in Fig. 8 together with their corresponding coefficients obtained via analytical amplitude-dependent stiffness method. It is found that the obtained damping coefficients by the analytical amplitude-dependent stiffness method and those obtained via numerical simulation are exactly similar and generate similar semicircular curves.

For further verification, the energy dissipation by the amplitude-independent physical damping matrix $\mathbf{D}$

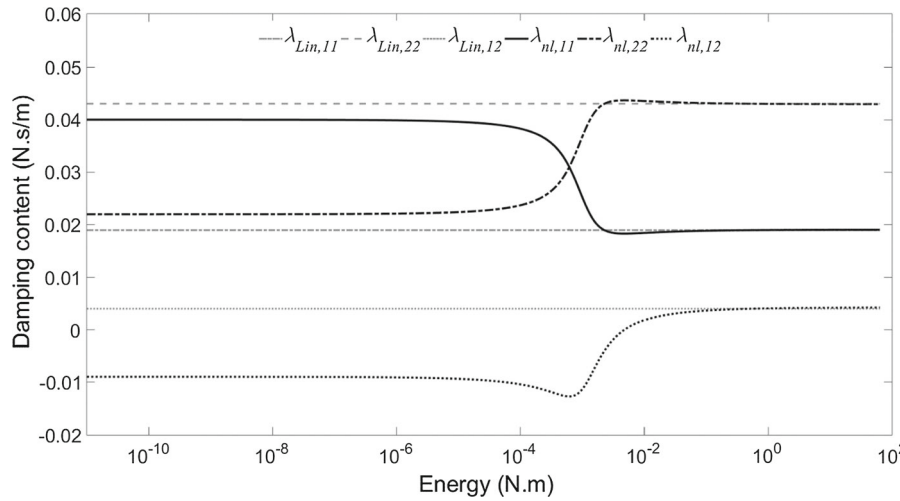

Fig. 4 Plots of damping coefficients of the amplitude-dependent modal damping matrix in Eq. (12b) at $p = 3$ and the amplitude-independent modal damping matrix in Eq. (15) for $p = 1$ versus the corresponding nonlinear energy in the nonlinear coupling spring

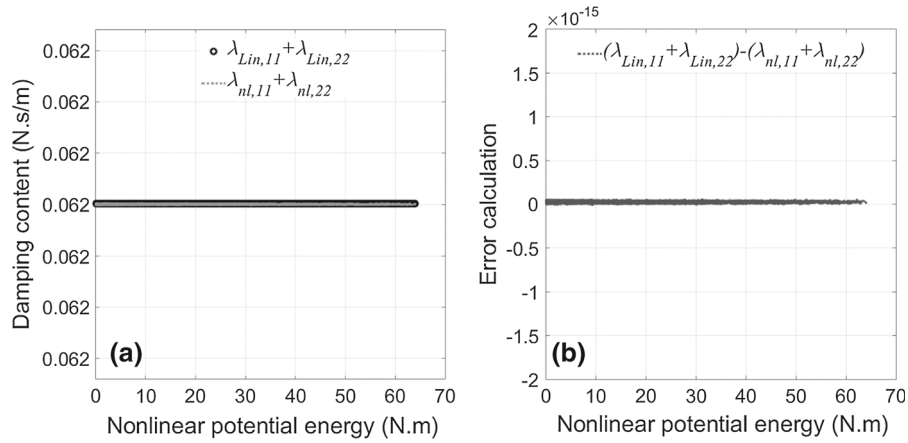

Fig. 5 Plots for the sum of diagonal damping coefficients of the amplitude-dependent modal damping matrix in Eq. (12b) at $p = 3$ and the amplitude-independent modal damping matrix in Eq. (15) for $p = 1$ versus the corresponding nonlinear energy in the nonlinear coupling spring in (**a**) and the corresponding error in (**b**)

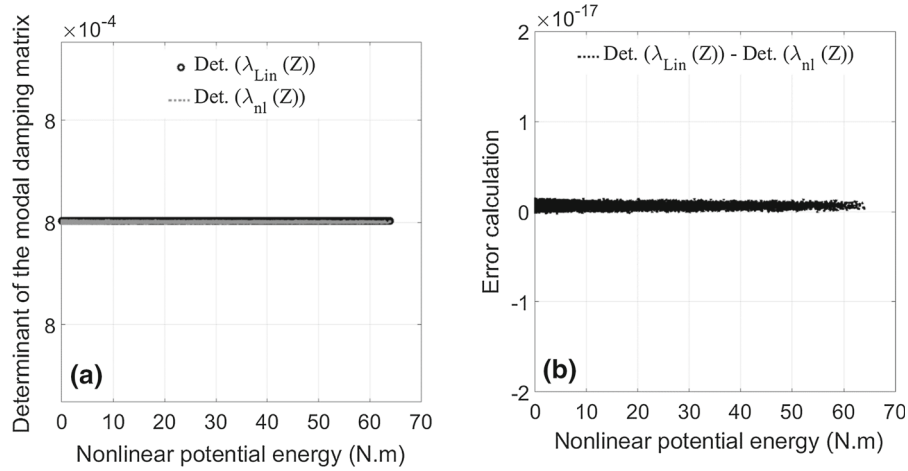

Fig. 6 Plots for determinants of the amplitude-dependent modal damping matrix in Eq. (12b) at $p = 3$ and the amplitude-independent modal damping matrix in Eq. (15) for $p = 1$ versus the corresponding nonlinear energy in the nonlinear coupling spring in (**a**) and the corresponding error in (**b**)

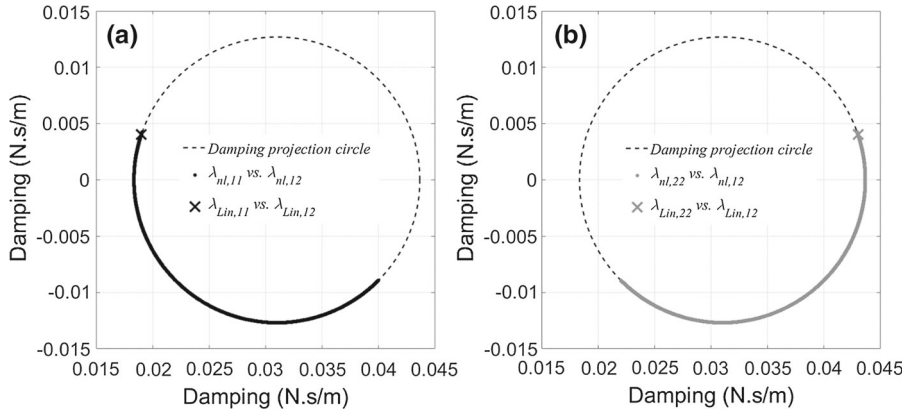

Fig. 7 Plots for the diagonal modal damping coefficients versus the anti-diagonal modal damping coefficient of the amplitude-dependent modal damping matrix in Eq. (12b) at $p = 3$ and the amplitude-independent modal damping matrix in Eq. (15) for $p = 1$

and that by the amplitude-dependent modal damping matrix $\boldsymbol{\lambda}_{\text{nl}}(Z)$ are calculated from

$$\begin{aligned} \boldsymbol{E}_{\text{diss}}(t) &= \dot{\mathbf{q}}(t)^{\text{T}}\ \mathbf{D}\ \mathbf{q}(t) \\ \bar{\boldsymbol{E}}_{\text{diss}}(t) &= \dot{\mathbf{y}}(t)^{\text{T}}\ \boldsymbol{\lambda}_{\text{nl}}(Z(t))\ \mathbf{y}(t) \end{aligned} \tag{18}$$

where the results are shown in Fig. 9. It is found that the curves of $\boldsymbol{E}_{\text{diss}}(t)$ and $\bar{\boldsymbol{E}}_{\text{diss}}(t)$ are exactly similar. This is also observed in Fig. 10 for the corresponding accumulated energy dissipation. Therefore, regardless of the odd power stiffness p value, the physical parameters of the system and the initial condition, the robustness of the analytical amplitude-dependent stiffness method in accurate prediction of damping and frequency variations is not affected. This method is directly applied into the equations of motion where the numerical simulation solution is not required to be known a priori.

5 Application with a nonnegative real-power coupling stiffness

The proposed amplitude-dependent stiffness method described in previous sections with examples is also applicable to nonlinear systems with a nonnegative real-power coupling stiffness (i.e, $p > 0$). Same derivation steps here and in [30] lead to the same formula for the scaling parameter δ, which was given in Eq. (1) at which amplitude-dependent stiffness is expressed by Eq. (5). For some values of nonnegative real-power stiffness, the results are shown in Fig. 11 for $p = 4/3$ at which $\delta = 1.0647$ and in Fig. 12 for $p = 2$ at which $\delta = 1.1953$ using similar initial condition and physical parameters of the previously considered LO-NES system. Exactly similar observations are obtained regarding modal damping variations under the effect of nonlinear potential energy change in the nonlinear spring. To avoid repetition, similar to the nonnegative odd-power stiffness in the LO-NES example in the previous section, the results for nonnegative real-power stiffness are found to be of the same robustness regardless of the initial condition and system physical parameters.

6 Application with two-story structure-NES system

Here, the real two-story structure-NES system in [32] is considered, which is shown in Fig. 13 to verify the robustness and applicability of the proposed amplitude-dependent stiffness method with real physical systems. The mass of the bottom floor of this structure is 24.3 kg, the mass of the top floor is 24.2 kg, and the mass of the NES is 2 kg.

The equations of motion of this structure-NES system are expressed in matrix form according to its identified physical parameters as

$$\mathbf{M}\,\ddot{\mathbf{x}} + \mathbf{D}\,\dot{\mathbf{x}} + \mathbf{K}\,\mathbf{x} = \mathbf{F} \tag{19}$$

where $\mathbf{M}$ is the mass matrix, $\mathbf{D}$ is the damping matrix, $\mathbf{K}$ is the stiffness matrix, $\mathbf{F}$ is the nonlinear coupling force vector, $\mathbf{x} = [x_1 \quad x_2 \quad x_3]^{\text{T}}$ is the vector of displacement, x_1 is the bottom floor displacement, x_2 is the top floor displacement, and x_3 is the NES mass displacement. The NES mass is coupled with the top floor via a nonlinear coupling cubic stiffness spring. This cubic stiffness is realized via a spring which is attached to be perpendicular to the oscillation direction of the structure as shown in Fig. 13. The matrices in Eq. (19) of

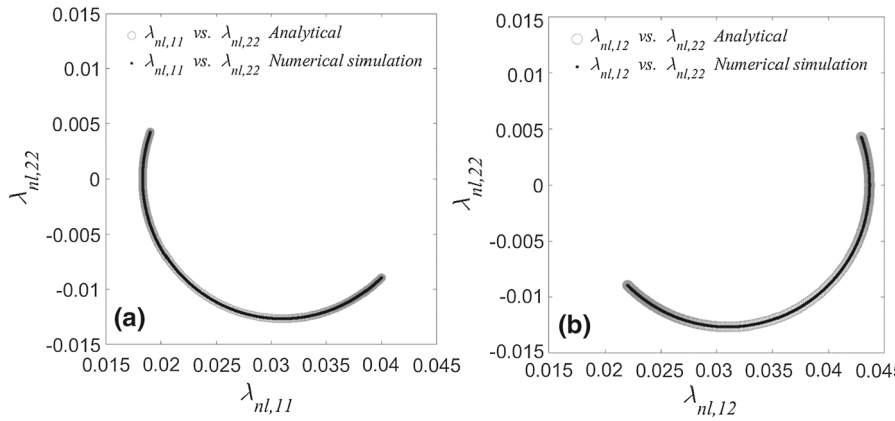

Fig. 8 Plots for analytical and numerical diagonal damping coefficients versus the anti-diagonal damping coefficient of the amplitude-dependent damping matrix in Eq. (12b) at $p = 3$, $u(0) = 0$, $v(0) = 4$, and $\dot{u}(0) = \dot{v}(0) = 0$

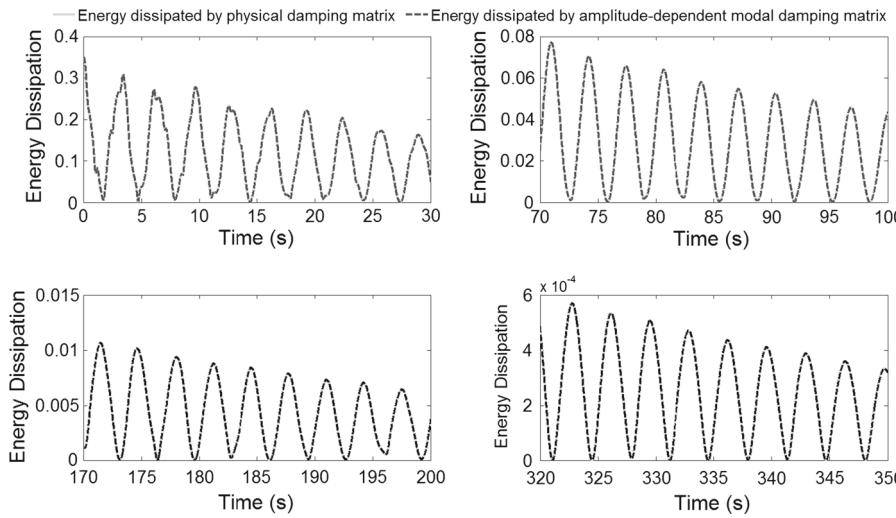

Fig. 9 Instantaneous energy dissipation by the physical amplitude-independent damping matrix **D** and the amplitude-dependent modal damping matrix $\boldsymbol{\lambda}_{\mathrm{nl}}(Z)$ versus the simulation time

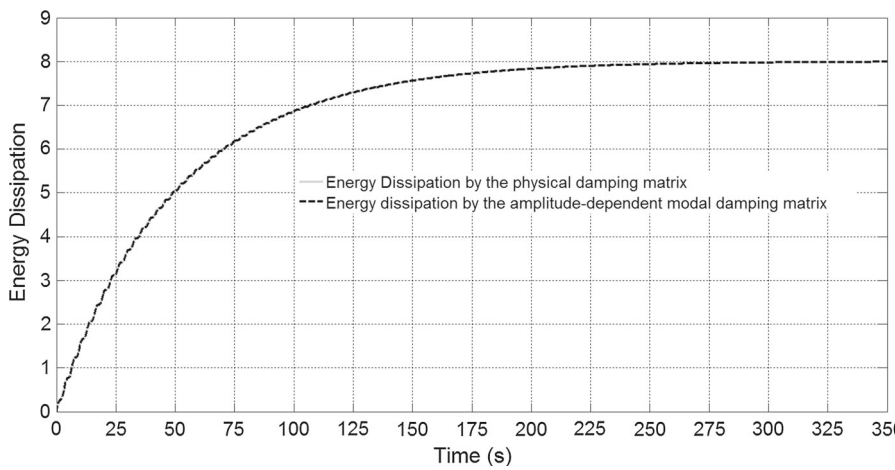

Fig. 10 Accumulated energy dissipation by the physical amplitude-independent damping matrix **D** and the amplitude-dependent modal damping matrix $\boldsymbol{\lambda}_{\mathrm{nl}}(Z)$ versus the simulation time

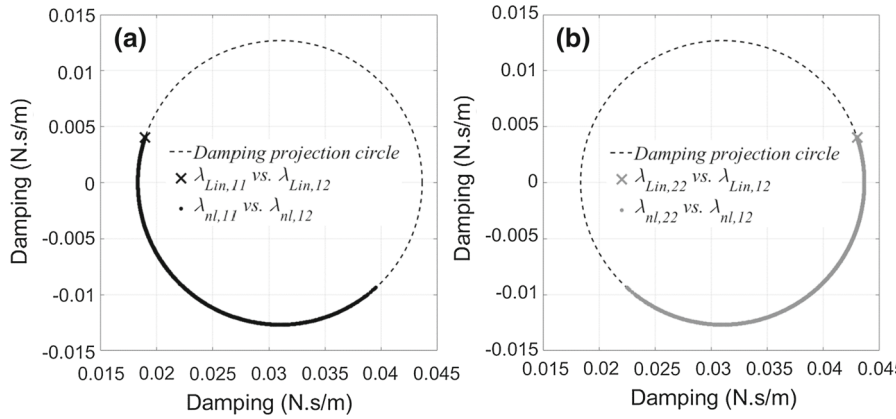

Fig. 11 Plots for the diagonal damping coefficients versus the anti-diagonal damping coefficient of the amplitude-dependent damping matrix in Eq. (13) at $p = 4/3$ and the amplitude-independent damping matrix in Eq. (15) for $p = 1$

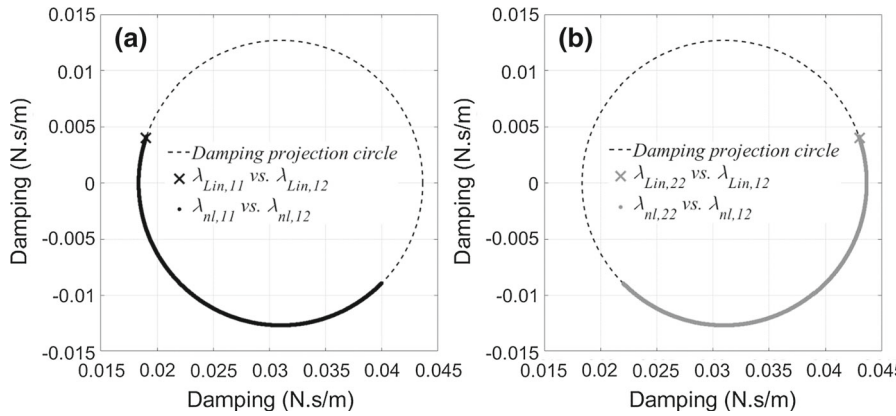

Fig. 12 Plots for the diagonal damping coefficients versus the anti-diagonal damping coefficient of the amplitude-dependent damping matrix in Eq. (13) at $p = 2$ and the amplitude-independent damping matrix in Eq. (15) for $p = 1$

the physical parameters of this structure-NES system in [32] at $p = 3$ are expressed as

$$\mathbf{M} = \begin{bmatrix} 24.3 & 0 & 0 \\ 0 & 24.2 & 0 \\ 0 & 0 & 2 \end{bmatrix} \text{kg},$$

$$\mathbf{K} = \begin{bmatrix} 15.04 & -8.22 & 0 \\ -8.22 & 8.22 & 0 \\ 0 & 0 & 0 \end{bmatrix} \times 10^3 \text{ N/m, and}$$

$$\mathbf{F} = \begin{bmatrix} 0 \\ k_{\text{nl}}\,(x_3 - x_2)^p \\ -k_{\text{nl}}\,(x_3 - x_2)^p \end{bmatrix} \text{N}$$

where the cubic stiffness coefficient is $k_{\text{nl}} = 3.2 \times 10^5$ N/m^3. However, the matrices of the physical parameters for the reference linear system at $p = 1$ which is employed with the amplitude-dependent stiffness method are expressed as

$$\mathbf{M} = \begin{bmatrix} 24.3 & 0 & 0 \\ 0 & 24.2 & 0 \\ 0 & 0 & 2 \end{bmatrix} \text{kg},$$

$$\mathbf{K} = \begin{bmatrix} 15.040 & -8.220 & 0 \\ -8.220 & 328.220 & -320 \\ 0 & -320 & 320 \end{bmatrix} \times 10^3 \text{ N/m, and}$$

$$\mathbf{F} = \begin{bmatrix} 0 \\ 0 \\ 0 \end{bmatrix} \text{N}$$

The physical damping matrix is the same for both cases of $p = 1$ and $p = 3$, which is expressed as

$$\mathbf{D} = \begin{bmatrix} 1.2155 & -0.2951 & 0 \\ -0.2951 & 2.9679 & -2.0000 \\ 0 & -2.0000 & 2.0000 \end{bmatrix} \text{N s/m}$$

The amplitude-dependent modal damping matrix for the nonlinear system at $p = 3$, which is analogous to that in Eq. (12b), is calculated according to the amplitude-dependent stiffness method at each value of Z as

$$\boldsymbol{\lambda}_{\text{nl}}(Z) = \boldsymbol{\Phi}(Z)^{\text{T}}\ \mathbf{M}^{-1/2}\mathbf{D}\mathbf{M}^{-1/2}\boldsymbol{\Phi}(Z) = \begin{bmatrix} \lambda_{\text{nl},11}(Z) & \lambda_{\text{nl},12}(Z) & \lambda_{\text{nl},13}(Z) \\ \lambda_{\text{nl},21}(Z) & \lambda_{\text{nl},22}(Z) & \lambda_{\text{nl},23}(Z) \\ \lambda_{\text{nl},31}(Z) & \lambda_{\text{nl},32}(Z) & \lambda_{\text{nl},33}(Z) \end{bmatrix} \quad (20)$$

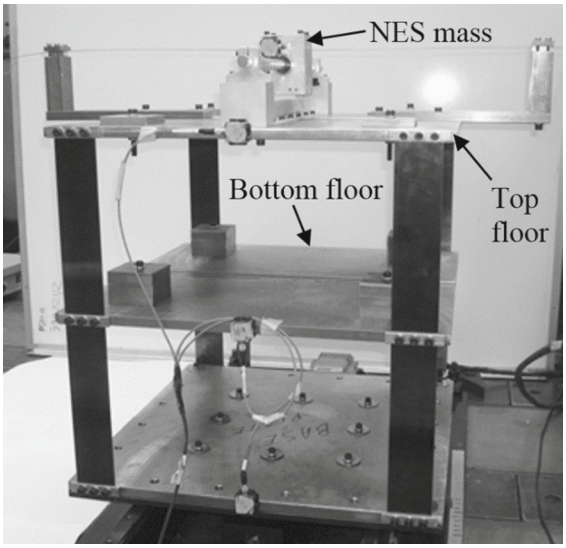

Fig. 13 Lab scale two-story dynamical structure-NES system [32]

The amplitude-independent modal damping matrix for the reference linear system at $p = 1$, which also is analogues to that in Eq. (15), is calculated as

$$\begin{aligned}\boldsymbol{\lambda}_{\mathrm{Lin}}(Z) &= \boldsymbol{\Phi}(Z)^{\mathrm{T}}\ \mathbf{M}^{-1/2}\mathbf{D}\mathbf{M}^{-1/2}\boldsymbol{\Phi}(Z)\\ &= \begin{bmatrix} \lambda_{\mathrm{Lin},11}(Z) & \lambda_{\mathrm{Lin},12}(Z) & \lambda_{\mathrm{Lin},13}(Z)\\ \lambda_{\mathrm{Lin},21}(Z) & \lambda_{\mathrm{Lin},22}(Z) & \lambda_{\mathrm{Lin},23}(Z)\\ \lambda_{\mathrm{Lin},31}(Z) & \lambda_{\mathrm{Lin},32}(Z) & \lambda_{\mathrm{Lin},33}(Z)\end{bmatrix}\\ &= \begin{bmatrix} 0.0301 & -0.0010 & 0.0070\\ -0.0010 & 0.0568 & 0.0078\\ 0.0070 & 0.0078 & 1.0857\end{bmatrix}\end{aligned} \tag{21}$$

The modal damping matrices in Eqs. (20) and (21) are always symmetric in modal coordinates. At the previously identified physical parameters, the results of diagonal modal damping coefficients and the absolute values of the anti-diagonal modal damping coefficients in Eq. (20) together with those of the reference linear system in Eq. (21) are plotted in Fig. 14 with respect to the nonlinear potential energy and in Fig. 15 with respect to the relative displacement of the NES mass. Similar to systems in the previous sections, the significant effect of nonlinear coupling stiffness in the system on modal damping content is clear in these figures.

It is also found here that all matrix similarity conditions between $\boldsymbol{\lambda}_{\mathrm{nl}}(Z)$ in Eq. (20) and $\boldsymbol{\lambda}_{\mathrm{Lin}}(Z)$ in Eq. (21) are satisfied such that both matrices have similar determinant, trace (sum of diagonal elements), rank, and eigenvalues. These findings of the real two-story structure-NES system strongly support the robustness of findings and conclusions obtained in previous sections for the two considered systems with arbitrary values of stiffness power, mass, damping, and stiffness. Unlike the considered systems in the previous sections, plotting diagonal modal damping coefficients against anti-diagonal coefficients should not necessarily produce a unique damping projection circle, since the system here has six different amplitude-dependent modal damping coefficients.

Again, Eq. (19) is used for numerical simulation to obtain the instantaneous energy dissipation $\boldsymbol{E}_{\mathrm{diss}}(t)$ in the physical structure-NES system using the linear physical damping matrix $\mathbf{D}$ and then by using the amplitude-dependent modal damping matrix in Eq. (20) to obtain the corresponding $\bar{\boldsymbol{E}}_{\mathrm{diss}}(t)$ for accuracy comparison. The obtained results are shown in Fig. 16a, where it is found that the curves of $\boldsymbol{E}_{\mathrm{diss}}(t)$ and $\bar{\boldsymbol{E}}_{\mathrm{diss}}(t)$ are exactly similar according to the error calculation in Fig. 16b. Therefore, regardless of the size of the system, the odd-power stiffness p value, physical parameters, and initial condition, the analytical amplitude-dependent stiffness method is again accurate in predicting damping variations in nonlinear dynamical systems.

The fundamental backbone branches in the FNEP in [30] have been obtained according to the time-dependent stiffness method where numerical integration of equations of motion was required. However, such backbone branches can be accurately obtained here using the amplitude-dependent stiffness method, where the solution via numerical integration is not required to be known a priori. Therefore, the three fundamental backbone branches for the considered two-story structure-NES system are obtained in Fig. 17 by plotting the frequencies calculated according to Eq. (8) with respect to the nonlinear potential energy $E_{\mathrm{pe}}^{\mathrm{nl}}(Z)$ given in Eq. (14). At the same figure, the exact frequencies obtained by the shooting method in [1–4] through the numerical integration of the original system in physical coordinates are also shown. Excellent agreement is observed between the backbones obtained by the proposed amplitude-dependent stiffness method with the exact backbones obtained by the shooting method via the numerical simulation.

Finally, it has been found through this study that the proposed method which is directly applied into the

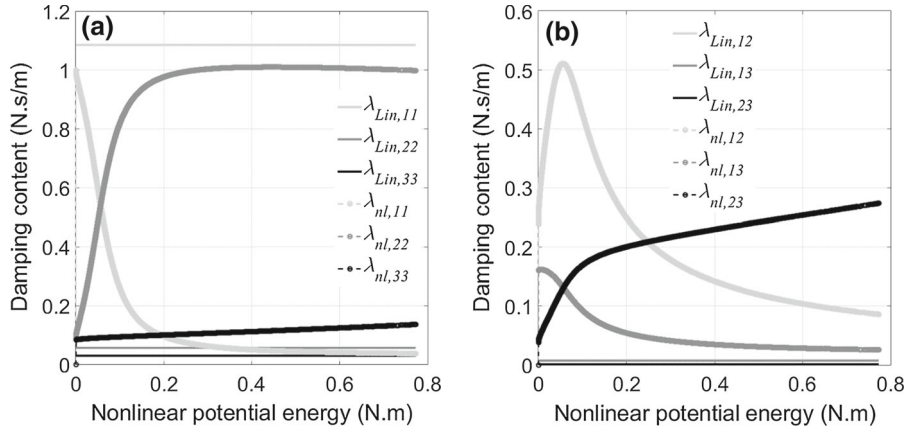

Fig. 14 Plots of damping coefficients for the amplitude-dependent modal damping matrix in Eq. (20) at $p = 3$ and the amplitude-independent modal damping matrix in Eq. (21) for $p = 1$ versus the corresponding nonlinear energy in the nonlinear coupling spring

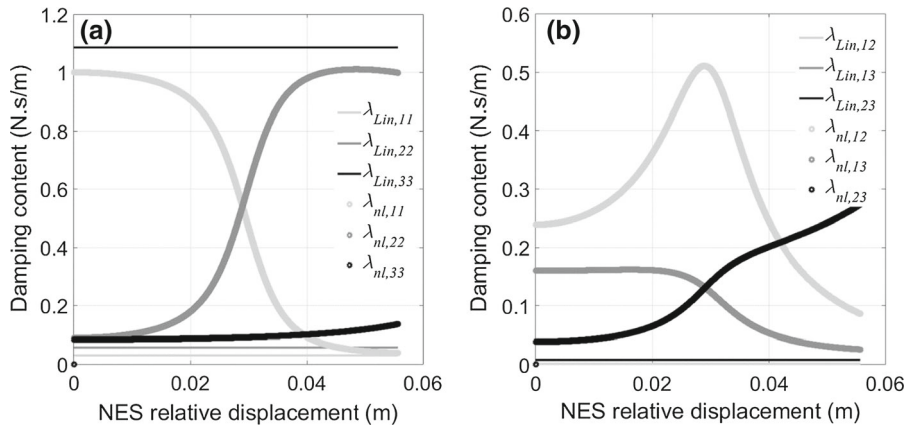

Fig. 15 Plots of damping coefficients for the amplitude-dependent modal damping matrix in Eq. (20) at $p = 3$ and the amplitude-independent modal damping matrix in Eq. (21) for $p = 1$ versus the corresponding relative displacement of the NES mass

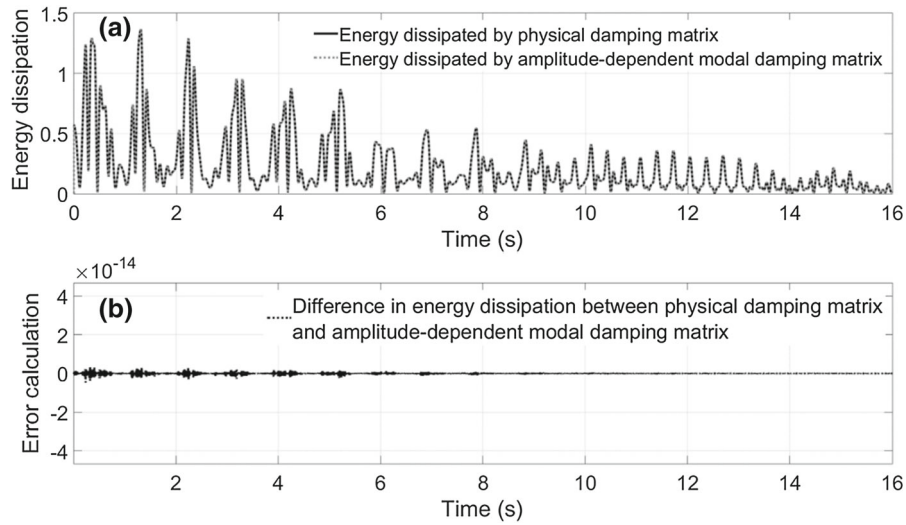

Fig. 16 Instantaneous energy dissipation by the physical amplitude-independent damping matrix **D** and the amplitude-dependent modal damping matrix $\boldsymbol{\lambda}_{\mathrm{nl}}(Z)$ versus the simulation time in (**a**) and the corresponding error calculation in (**b**)

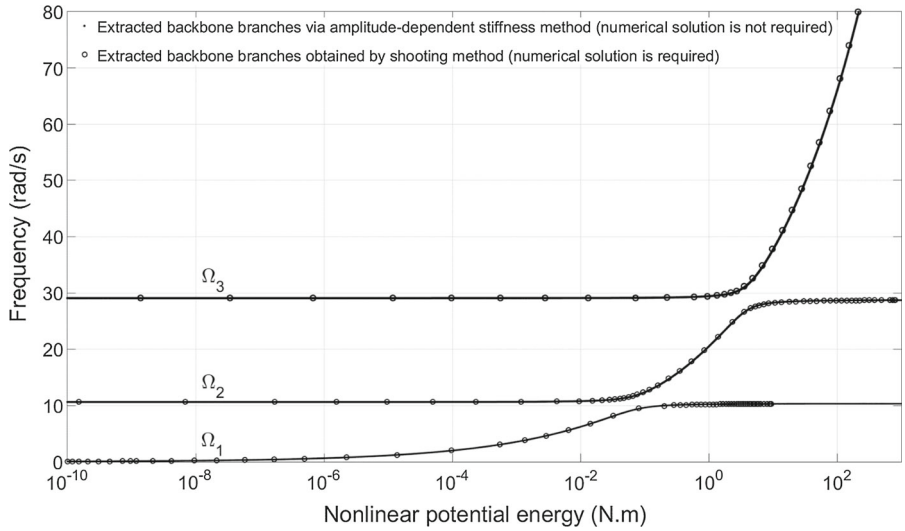

Fig. 17 Exact and amplitude-dependent stiffness fundamental backbone branches versus the energy in the nonlinear coupling spring for the two-story structure-NES system

equations of motion of nonlinear systems (the solution is not required to be known a priori) is capable of providing significant information about the nonlinear dynamical behavior in modal damping content and nonlinear frequencies.

7 Concluding remarks

Amplitude-dependent stiffness method is employed here for studying dependence of modal damping content on nonlinear energy content in nonlinear dynamical systems. The method is directly applied into the equations of motion of the considered dynamical systems where the numerical simulation solution is not required to be known a priori. The success of application of the proposed method is based on finding the scaling parameter to the amplitude-dependent stiffness, which significantly helped in studying the effect of nonlinear stiffness on modal damping content of such nonlinear dynamical systems. Accordingly, several new findings have been reached regarding modal damping content variations under the effect of appearance of nonlinear coupling stiffness in the considered systems. The robustness of the proposed analytical method in determining the energy-dependent modal damping and frequencies has been verified via numerical simulation for three different considered examples. The comparison between analytical and numerical simulation results show that the proposed analytical method is very close to be exact in predicting the effect of nonlinear energy content within the system on both modal damping and modal frequencies.

Compliance with ethical standards

Conflict of interest The authors declare that they have no conflict of interest.

References

1. Vakakis, A.F., Gendelman, O.V., Kerschen, G., Bergman, L.A., McFarland, D.M., Lee, Y.S.: Nonlinear Targeted Energy Transfer in Mechanical and Structural Systems I and II. Springer, Berlin (2008)
2. Peeters, M., Viguié, R., Sérandour, G., Kerschen, G., Golinval, J.C.: Nonlinear normal modes, part II: toward a practical computation using numerical continuation techniques. Mech. Syst. Signal Process. **23**(1), 195–216 (2009)
3. Kerschen, G., Peeters, M., Golinval, J.C.: Nonlinear normal modes, part I: a useful framework for the structural dynamicits. Mech. Syst. Signal Process. **23**, 170–194 (2009)
4. Renson, L., Kerschen, G., Cochelin, B.: Numerical computation of nonlinear normal modes in mechanical engineering. J. Sound Vib. **364**, 177–206 (2016)
5. Salenger, G., Vakakis, A.F., Gendelman, O., Manevitch, L., Andrianov, I.: Transitions from strongly to weakly nonlinear motions of damped nonlinear oscillators. Nonlinear Dyn. **20**(2), 99–114 (1999)
6. Nayfeh, A.H.: Perturbation Methods. Wiley, New York (1973)
7. Nayfeh, A.H., Mook, D.T.: Nonlinear Oscillations. Wiley, New York (1979)
8. Luo, A.C.J., Huang, J.: Approximate solutions of periodic motions in nonlinear systems via a generalized harmonic balance. J. Vib. Control **18**(11), 1661–1674 (2011)
9. Beléndez, A., Hernández, A., Márquez, A., Beléndez, T., Neipp, C.: Analytical approximations for the period of a nonlinear pendulum. Eur. J. Phys. **27**(3), 539–551 (2006)

10. Beléndez, A., Hernández, A., Beléndez, T., Álvarez, M.L., Gallego, S., Ortuño, M., Neipp, C.: Application of the harmonic balance method to a nonlinear oscillator typified by a mass attached to a stretched wire. J. Sound Vib. **302**(4–5), 1018–1029 (2007)
11. Sun, W.P., Wu, B.S., Lim, C.W.: Approximate analytical solutions for oscillation of a mass attached to a stretched elastic wire. J. Sound Vib. **300**(3), 1042–1047 (2007)
12. Durmaz, S., Demirbağ, S.A., Kaya, M.O.: Approximate solutions for nonlinear oscillation of a mass attached to a stretched elastic wire. Comput. Math. Appl. **61**(3), 578–585 (2011)
13. Mickens, R.E.: Comments on the method of harmonic balance. J. Sound Vib. **94**, 456–460 (1984)
14. Beléndez, A., Beléndez, T., Márquez, A., Neipp, C.: Application of He's homotopy perturbation method to conservative truly nonlinear oscillators. Chaos Solitons Fractals **37**(3), 770–780 (2008)
15. Cveticanin, L.: Homotopy-perturbation method for pure nonlinear differential equation. Chaos Solitons Fractals **30**(5), 1221–1230 (2006)
16. Beléndez, A., Beléndez, T., Neipp, C., Hernández, A., Álvarez, M.L.: Approximate solutions of a nonlinear oscillator typified as a mass attached to a stretched elastic wire by the homotopy perturbation method. Chaos Solitons Fractals **39**(2), 746–764 (2009)
17. Cveticanin, L.: Analytical methods for solving strongly nonlinear differential equations. J. Sound Vib. **214**(2), 325–338 (1998)
18. Cveticanin, L.: Pure odd-order oscillators with constant excitation. J. Sound Vib. **330**(5), 976–986 (2011)
19. Brennan, M.J., Kovacic, I., Carrella, A., Waters, T.P.: On the jump-up and jump-down frequencies of the Duffing oscillator. J. Sound Vib. **318**(4), 1250–1261 (2008)
20. Burton, T.D.: On the amplitude decay of strongly non-linear damped oscillators. J. Sound Vib. **87**(4), 535–541 (1983)
21. Yuste, S.B., Bejarano, J.D.: Amplitude decay of damped non-linear oscillators studied with Jacobian elliptic functions. J. Sound Vib. **114**(1), 33–44 (1987)
22. Mickens, R.E.: A generalized iteration procedure for calculating approximations to periodic solutions of truly nonlinear oscillators. J. Sound Vib. **287**(4–5), 1045–1051 (2005)
23. AL-Shudeifat, M.A.: Analytical formulas for the energy, velocity and displacement decays of purely nonlinear damped oscillators. J. Vib. Control **21**(6), 1210–1219 (2013)
24. Andrianov, I.V., Awrejcewicz, J.: Asymptotical behavior of a system with damping and high power-form non-linearity. J. Sound Vib. **267**, 1169–1174 (2003)
25. Gottlieb, H.P.W.: Frequencies of oscillators with fractional-power non-linearities. J. Sound Vib. **261**(3), 557–566 (2003)
26. Cveticanin, L.: Oscillator with fraction order restoring force. J. Sound Vib. **320**(4), 1064–1077 (2009)
27. Rakaric, Z., Kovacic, I.: Approximations for motion of the oscillators with a non-negative real-power restoring force. J. Sound Vib. **330**(2), 321–336 (2011)
28. Al-Shudeifat, M.A.: Amplitudes decay in different kinds of nonlinear oscillators. J. Vib. Acoust. **137**(3), 031012 (2015)
29. Al-Shudeifat, M.A.: Approximation of the frequency-energy dependence in the nonlinear dynamical systems. In: ASME 2016 International Design Engineering Technical Conferences and Computers and Information in Engineering Conference No. DETC2016-60163, pp. V006T09A042–V006T09A042 (2016)
30. Al-Shudeifat, M.A.: Time-varying stiffness method for extracting the frequency-energy dependence in the nonlinear dynamical systems. Nonlinear Dyn. **89**(2), 1463–1474 (2017)
31. AL-Shudeifat, M.A.: Amplitude-dependent stiffness method for studying frequency and damping variations in nonlinear dynamical systems. In: ASME 2017 International Design Engineering Technical Conferences and Computers and Information in Engineering Conference No. DETC2017-67918, pp. V006T10A047–V006T10A047 (2017)
32. Quinn, D.D., Hubbard, S., Wierschem, N., Al-Shudeifat, M.A., Ott, R.J., Luo, J., Spencer Jr., B.F., McFarland, D.M., Vakakis, A.F., Bergman, L.A.: Equivalent modal damping, stiffening and energy exchanges in multi-degree-of-freedom systems with strongly nonlinear attachments. Proc. Inst. Mech. Eng. K J. Multi-body Dyn. **226**(2), 122–146 (2012)